# Preparation, Characterisation and Electrical Conductivity studies of Nanocrystalline $BaMoO_4$ material.

N. Nallamuthu[1], I. Prakash[1], M. Venkateswarlu[2], N. Satyanarayana[*1]
[1] Department of Physics, Pondicherry University, Puducherry. 605 014, India
[2]Research and Engineering center, Amara Raja Batteries Ltd, Tirupati-517520, AP, India.

## Abstract

Nanocrystalline $BaMoO_4$ powder of scheelite type was prepared by acrylamide assisted sol-gel combustion process. The dried gel, prepared at 60 $^oC$, was heated at different temperatures and characterized through XRD, FTIR, TG-DTA and SEM-EDAX techniques. Crystalline phase identification and crystallite size (~60 nm) calculation were made from the observed XRD patterns of the $BaMoO_4$ powder. The structure and thermal behavior of the nanocrystalline $BaMoO_4$ powder was identified respectively through FTIR and TG-DTA measurements. For the sintered $BaMoO_4$ pellets, electrical conductivity of grain and grain boundary effects were evaluated from the measured impedance data at different temperatures.

***Key words:*** Combustion Process; scheelite type nanocrystalline oxide; XRD; FTIR; TG-DTA; SEM-EDAX; Impedance; Electrical conductivity.

## 1. Introduction

Generally, Oxygen ion conductors are much imperative materials and can be used intensively in various devices such as solid oxide fuel cells, oxygen sensors, electrochemical oxygen pumps, etc. [1-2]. Several families of oxygen ion conductors are being investigated for intermediate temperature solid oxide fuel cells (ITSOFCs) like fluorite type (stabilized $ZrO_2$, $CeO_2$ and $\delta$-$Bi_2O_3$), pervoksite type ($LaGaO_3$, $BaCeO_3$ and $SrCeO_3$), brownmillerite type ($Ba_2In_2O_3$), Aurivillius type (BIMEVOX), pyrochlore type ($Gd_2Zr_2O_7$), scheelite type ($PbWO_4$) , etc. [3-5].

Among the above, scheelite type oxides exhibit high ion conductivity, which is comparable with the yttria stabilized zirconia. Takao Esaka et al. systematically investigated the composition dependent of electrical conductivity for $PbWO_4$ scheelite type materials and found the higher electrical conductivity of $4.2\times10^{-2}$ $Scm^{-1}$ at 800 $^oC$ for $Pb_{0.8}La_{0.2}WO_{4.1}$. V.Thangadurai et al. preapared scheelite type $ABO_4$ (A= Ca, Sr, Ba; B= Mo,W) materials and reported that $PbWO_4$ and $SrWO_4$ show the higher electrical conductivity between the 500 $^oC$ to 900 $^oC$ temperatures [7].

The nanocrystalline metal oxide compounds have the small grain size, which may lead to the increase of ionic conductivity and also the stabilization of crystal structure at higher temperatures. In recent years, nanostructured ceramics have been extensively investigated and it exhibit enhanced electrical, magnetic, mechanical, optical, sensing, and biomedical properties because of the large fraction of grain boundaries effects, compared with their respective micro structured materials [8]. In the presence study, scheelite type nanocrystalline $BaMoO_4$ powder was prepared using acrylamide assisted sol-gel combustion process and it was characterized by XRD, FTIR, TG-DTA and SEM – EDAX. Also, for the sintered $BaMoO_4$ pellets, electrical conductivity of grain and grain boundary effects were evaluated from the measured impedance data at different temperatures.

## 2. Experimental

### 2.1. Sol-gel combustion process

Nanocrystalline $BaMoO_4$ powder was synthesized by acrylamide based combustion process using Acrylamide and citric acid as fuels. The precursor chemicals (Barium nitrate and Ammonium molybdate) were taken according to their respective molecular weight percentages. Barium nitrate is dissolved in distilled water and mixed with citric acid and acrylamide under continuous stirring. Ammonium molybdate is added to the distilled water and stirred the solution for half an hour to become the transparent solution. Ammonium molybdate solution is added to the barium nitrate solution and stirring continuously till the formation of the gel. The prepared gel was dried and calcined at various temperatures 60 $^oC$, 150 $^oC$, 250 $^oC$, 350 $^oC$, 500 $^oC$, 600 $^oC$, 700 $^oC$, 800 $^oC$ and 900 $^oC$. All the calcined $BaMoO_4$ samples were characterized by FTIR technique.

#### 2.2: TG-DTA , XRD and FTIR measurements

The thermal behavior of the sample was recorded using TA instruments SDT Q600 V20.5 DTA-TGA thermal analyser. The fine powdered dried gel sample of 9.3 mg was placed in the alumina crucible heated at the rate of 10 $^oC$ per minute from 40 $^oC$ to 900 $^oC$ under nitrogen atmosphere. XRD patterns were recorded, for the fine powdered dried gels, using panalytical X'pert pro diffractometer with Cu $K_\alpha$ as the source radiation of wavelength $\lambda$=1.4158 $A^o$. The fine powdered mixture of calcined gel sample, for different calcined temperatures,

and KBr powder in 1:20 ratio were made in to thin transparent pallets using KBr press. FTIR spectra were recorded for the thin transparent pallets using Schimadzu FTIR/8300/8700 spectrophotometer between 4000 – 400 $cm^{-1}$ with 2 $cm^{-1}$ resolution for 20 scans. The synthesized nanocrystalline BaMoO4 powder was pressed into 10mm diameter and 2-3 mm thickness pellet at 5000 $kg/cm^2$ using KBr press. The shape and size of the prepared $BaMoO_4$ sintered powder and pellet samples at various temperatures were investigated using a scanning electron microscope (SEM), JEOL-JSM6400 scanning electron microscope with an accelerating voltage of 20 keV. The nanocrystalline $BaMoO_4$ pellet sample was sintered at various temperatures to calculate the relative density and also to measure the impedance.

## 3. Results and discussion:

### 3.1 TG-DTA

Fig. 1 shows the TG-DTA thermogram of nanocrystalline $BaMoO_4$ gel sample. The observed wide endothermic peak between 40 $^oC$ and 550 $^oC$ for the dried gel is due to the evaporation of water molecules and other organic residues existing in the sample, which also are confirmed from the FTIR results.

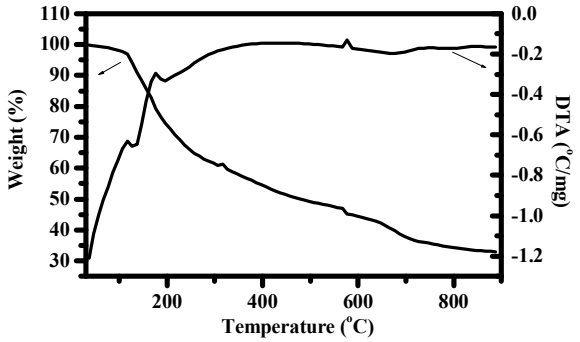


Fig.1 TG-DTA curve for the $BaMoO_4$ gel sample dried at 60 $^oC$.

The exothermic peak observed at 577 $^oC$ in DTA curve may corresponds to the formation of crystalline $BaMoO_4$ phase and the corresponding weight loss is observed in the TG curve. Further, the crystalline $BaMoO_4$ phase is also confirmed from the XRD results.

### 3.2 FTIR

Fig. 2 shows the FTIR spectra recorded for the $BaMoO_4$ dried gel samples calcined at different temperatures 60 $^oC$, 150 $^oC$, 250 $^oC$, 350 $^oC$, 500 $^oC$, 600 $^oC$, 700 $^oC$, 800 $^oC$ and 900 $^oC$. From Fig. 2, the observed major bands are 3440, 3210,1650, 1390, 1220, 1050, 903 and 850 $cm^{-1}$. The IR bands at 3440 and 1650 $cm^{-1}$ are respectively, attributed to stretching and bending vibrational modes of O-H of molecular water and 3210 $cm^{-1}$ is due to stretching vibration mode of the O-H and N-H bond. The band at 1390 $cm^{-1}$ is corresponds to the symmetric and asymmetric stretching vibration of $COO^-$ groups and formation of ammonium carboxylate. The IR bands at 1220 & 1050 $cm^{-1}$ is formed due to $CO_3^{2-}$ functional groups indicate the formation of carboxylate. The observed bands at 903 and 850 $cm^{-1}$ are due to the Mo-O stretching vibration and are attributed to the formation of $MoO_3$ in $BaMoO_4$ sample.

For higher calcined temperature, The FTIR spectra of the sample showed a decrease in the intensity of the bands at 3405 & 1620 $cm^{-1}$, 3210, 1390, 1220, 1050 $cm^{-1}$, which are due to the removal of molecular water from the sample and also removal of existing organic residues. The appearance of the bands at 903 and 850 $cm^{-1}$ are corresponding to the formation of $MoO_3$ in $BaMoO_4$ sample, which are confirmed by TG-DTA and XRD results.

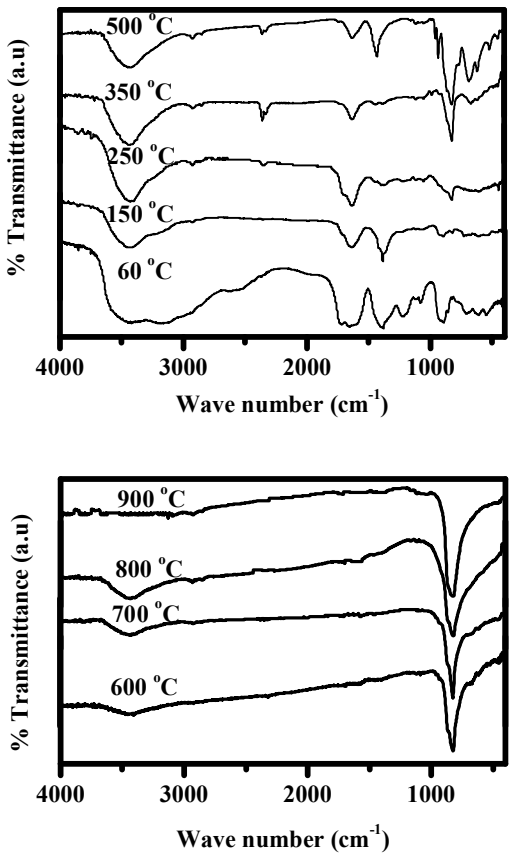


Fig.2 FTIR spectra for the $BaMoO_4$ gel sample heated at various temperatures.


NSTI-Nanotech 2009, www.nsti.org, ISBN 978-1-4398-1782-7 Vol. 1, 2009

## 3.3 XRD

Fig 3. shows the XRD patterns of the $BaMoO_4$ sample obtained at different calcined temperatures. The observed crystalline peaks in the XRD patterns are compared with the standard ICDD 00-029- 0193 data and confirmed the formation of the scheelite type $BaMoO_4$ crystalline phase. The crystalline size of the $BaMoO_4$ sample is calculated using scherer's formula: $D = 0.9\lambda / (\beta \cos\theta)$, where $\lambda$ is the X-ray wave length (0.15418 nm), $\beta$ is full width half maximum (FWHM) of the peak. The crystalline size of $BaMoO_4$ is found to be ~60nm.

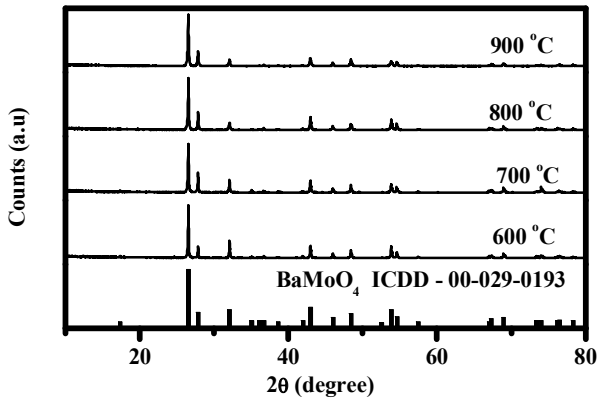


Fig.3 XRD patterns for the $BaMoO_4$ gel sample heated at various temperatures.

## 3.4 SEM-EDAX measurements

SEM images of the $BaMoO_4$ powder, heated at various temperature from 600 °C to 900 °C is shown in fig. 4. SEM micrographs showed an agglomerated spherical particles of $BaMoO_4$ sintering at various temperatures and their particle sizes are found to be ~100 to ~300nm.

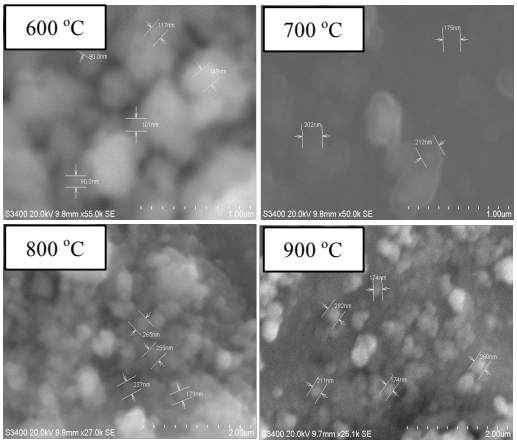


Fig 4.SEM images of $BaMoO_4$ powder heated at different temperatures.

The SEM image and relative density of the $BaMoO_4$ pellets sintered at various temperatures are shown in fig 5. The relative density is calculated using the mass and thickness of the $BaMoO_4$ sintered pellets. The relative density increases with increasing the sintered temperature from 600 °C to 900 °C. The relative density of $BaMoO_4$ sintered pellet at 900 °C is 91.5% of theoretical density. The sintering behaviour of the sample is also investigated by SEM at different temperatures (600 °C - 900 °C). The size of the grain is increased with increasing the sintering temperature.

SEM–EDAX spectrum are respectively confirm the existence and uniform distribution of O, Mo and Ba in the $BaMoO_4$. SEM- EDAX results confirm the formation of the $BaMoO_4$, and it is free from organic contamination.

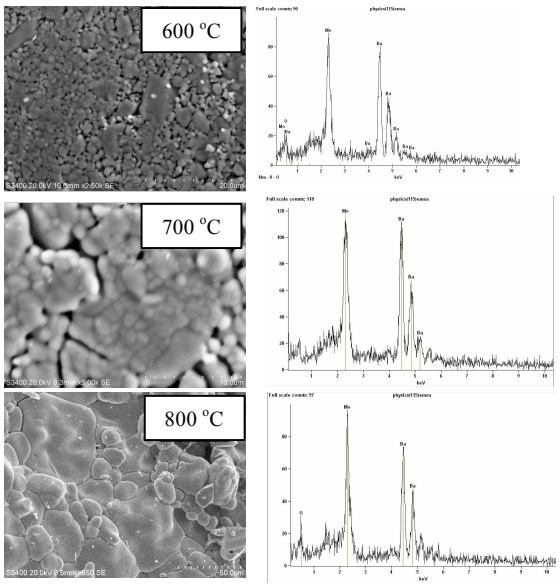


Fig 5. SEM image and EDAX of $BaMoO_4$ sintered pellets at different temperatures.

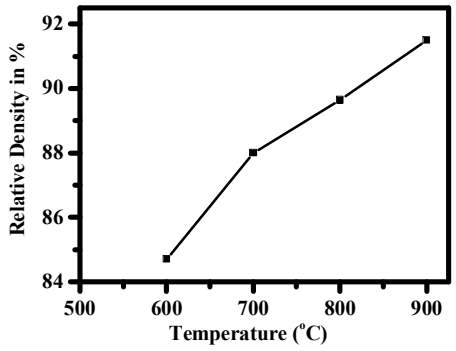


Fig 6.Relative density of sintered $BaMoO_4$ pellets at different temperatures.

| Element Line | Net Counts | Weight % | Atom % | Formula |
|---|---|---|---|---|
| O K | 59 | 18.99S | 63.99 | |
| Mo K | 20 | --- | --- | |
| Mo L | 1514 | 24.90 | 13.99 | $MoO_3$ |
| Mo M | 129 | --- | --- | |
| Ba L | 1854 | 56.11 | 22.02 | BaO |
| Ba M | 58 | --- | --- | |
| Total | | 100.00 | 100.0 | |

Table 1.: Weight percentage of each element (Ba,Mo and O) for SEM-EDAX result of $BaMoO_4$ pellet, Sintered at 800 $^oC$.

## 3.5 Electrical conductivity

For the nanocrystalline BaMoO4 sintered pellets at different temperatures, Electrical conductivity of grain and grain boundary effects were evaluated from the measured impedance data. Fig 8. shows the heating and cooling Log σT vs 1000/T plots of nanoocrystalline $BaMoO_4$. The activation energy is calculated from the Log σT vs 1000/T plot of $BaMoO_4$ crystalline materials and it is found to be 0.649eV for grain interior conductivity for heating and 0.7973 eV for cooling.

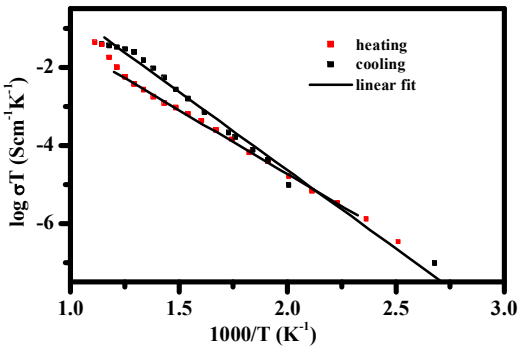


Fig 8. Heating and cooling Log σT vs 1000/T plots of nanocrystalline $BaMoO_4$.

## 4. Conclusion

Nanocrystalline $BaMoO_4$ powder was synthesized using acrylamide assisted combustion process. Thermogram of the BaMoO4 showed the complete crystallization at 577 $^oC$. XRD pattern confirmed the formation of the crystalline phase of the scheelite type $BaMoO_4$ and the calculated crystalline size is found to be ~60nm, using the Scherer's formula. Formation of $MoO_3$ is identified by FTIR spectra. SEM micrograph showed an agglomerated spherical particles of $BaMoO_4$ sintering at various temperatures and their measured particle sizes is found to be ~100 to ~300nm. SEM–EDAX spectrum are respectively confirm the existence and uniform distribution of O, Mo and Ba in the $BaMoO_4$. The relative density of the sintered $BaMoO_4$ pellet at 900 $^oC$ is found to be 91.5% of theoretical density. The bulk conductivity of $BaMoO_4$, sintered at 900 $^oC$, is 2.1 x $10^{-5}$ $Scm^{-1}$.


## Acknowledgement:

Dr NS is gratefully acknowledged CSIR, DRDO, AICTE and DST, Govt of India, for receiving the financial support in the form of major research projects. NN acknowledge CSIR-SRF for receiving fellowship for doing Ph.D.


## References


[1] J.P.P. Huijsmans, Curr. Opin. Solid State Mater. Sci., 5, 317, (2001) .
[2] P.N. Dyer, R.E. Richards, S.L. Russek, D.M. Taylor, Solid State Ionics, 134, 21, (2000).
[3] John B. Goodenough, Annu. Rev. Mater. Res.,. 33, 91,2003.
[4] V.V. Khartona, F.M.B. Marquesa, A. Atkinson, Solid State Ionics, 174, 135, (2004).
[5] GGZhang, Q F Fang1, X PWang and ZGYi, J. Phys.: Condens. Matter, 15, 4135, 2003.
[6] T.Esaka, Solid state ionics 136-137,1,2000.
[7] V. Thangadurai, S.Knilllmayer,W.Weppner, Material science and engineering B, 106,228,2004.
[8] Martin G.Bellino, Diego G.Lamas and Noemi E.Walsoe de Reca, Adv. Funct. Mater., 16, 107, 2006.